


## Growth diagram of AlN epilayers grown by plasma-assisted molecular beam epitaxy

Huan Liu(刘欢), Pengfei Shao(邵鹏飞), Yu Liu(柳裕), Qi Yao(姚齐), Tao Tao(陶涛), Zili Xie(谢自力), Dunjun Chen(陈敦军), Bin Liu(刘斌), Hai Lu(陆海), Rong Zhang(张荣), Ke Wang(王科)

**Citation:**Chin. Phys. B, 2025, 34 (**7**): 077701. DOI: 10.1088/1674-1056/adcb23
http://cpb.iphy.ac.cn; http://iopscience.iop.org/cpb

**What follows is a list of articles you may be interested in**

---

## Normally-off AlGaN/GaN heterojunction field-effect transistors with *in-situ* AlN gate insulator

Taofei Pu(蒲涛飞), Shuqiang Liu(刘树强), Xiaobo Li(李小波), Ting-Ting Wang(王婷婷), Jiyao Du(都继瑶), Liuan Li(李柳暗), Liang He(何亮), Xinke Liu(刘新科), and Jin-Ping Ao(敖金平)

Chin. Phys. B, 2022, 31 (**12**): 127701. DOI: 10.1088/1674-1056/ac7a0e

## Epitaxy of III-nitrides on two-dimensional materials and its applications

Yu Xu(徐俞), Jianfeng Wang(王建峰), Bing Cao(曹冰), and Ke Xu(徐科)

Chin. Phys. B, 2022, 31 (**11**): 117702. DOI: 10.1088/1674-1056/ac921f

## Monolithic epitaxy and optoelectronic properties of single-crystalline *γ*-$In_2Se_3$ thin films on mica

Xibo Yin(尹锡波), Yifan Shen(沈逸凡), Chaofan Xu(徐超凡), Jing He(贺靖), Junye Li(李俊烨), Haining Ji(姬海宁), Jianwei Wang(王建伟), Handong Li(李含冬), Xiaohong Zhu(朱小红), Xiaobin Niu(牛晓滨), and Zhiming Wang(王志明)

Chin. Phys. B, 2021, 30 (**1**): 017701. DOI: 10.1088/1674-1056/abcf32

## Fabrication and characterization of one-port surface acoustic wave resonators on semi-insulating GaN substrates

Xue Ji(吉雪), Wen-Xiu Dong(董文秀), Yu-Min Zhang(张育民), Jian-Feng Wang(王建峰), Ke Xu(徐科)

Chin. Phys. B, 2019, 28 (**6**): 067701. DOI: 10.1088/1674-1056/28/6/067701

## Observation of positive and small electron affinity of Si-doped AlN films grown by metalorganic chemical vapor deposition on n-type 6H-SiC

Feng Liang(梁锋), Ping Chen(陈平), De-Gang Zhao(赵德刚), De-Sheng Jiang(江德生), Zhi-Juan Zhao(赵志娟), Zong-Shun Liu(刘宗顺), Jian-Jun Zhu(朱建军), Jing Yang(杨静), Wei Liu(刘炜), Xiao-Guang He(何晓光), Xiao-Jing Li(李晓静), Xiang Li(李翔), Shuang-Tao Liu(刘双韬), Hui Yang(杨辉), Li-Qun Zhang(张立群), Jian-Ping Liu(刘建平), Yuan-Tao Zhang(张源涛), Guo-Tong Du(杜国同)

Chin. Phys. B, 2016, 25 (**5**): 057703. DOI: 10.1088/1674-1056/25/5/057703

---

# Growth diagram of AlN epilayers grown by plasma-assisted molecular beam epitaxy

Huan Liu(刘欢)[1], Pengfei Shao(邵鹏飞)[1,2,†], Yu Liu(柳裕)[1], Qi Yao(姚齐)[1], Tao Tao(陶涛)[1], Zili Xie(谢自力)[1], Dunjun Chen(陈敦军)[1], Bin Liu(刘斌)[1], Hai Lu(陆海)[1,2], Rong Zhang(张荣)[1,2,3], and Ke Wang(王科)[1,2,‡]

[1] *Jiangsu Provincial Key Laboratory of Advanced Photonic and Electronic Materials, School of Electronic Science and Engineering, Nanjing University, Nanjing* 210093, *China*
[2] *Hefei National Laboratory, Hefei* 230088, *China*
[3] *Xiamen University, Xiamen* 361005, *China*

(Received 4 March 2025; revised manuscript received 7 April 2025; accepted manuscript online 10 April 2025)

We have investigated homoepitaxy of AlN films grown by molecular beam epitaxy (MBE) on AlN/sapphire templates. The MBE epitaxy of AlN at the low temperature range, which is suitable for AlGaN, encounters significant challenge in preventing Al droplet and pits, since the migration and desorption rate of Al atom are very low. In contrast, by elevating the growth temperature, such a difficulty can be effectively overcome, and we were able to grow AlN films with much improved surface morphology and obtained step flow growth mode without any Al droplets and pits. The cathodoluminescence spectroscopy indicate that the impurity incorporation and defect generation in the AlN epilayers was suppressed by elevating the growth temperature. A systematic investigation on the influence of Al beam flux and growth temperature in a very wide range on the AlN films has been conducted, and a comprehensive growth diagram of MBE AlN has been obtained.

**Keywords:** AlN, epitaxy, films morphology, growth diagram

**PACS:** 77.55.hd, 81.15.–z, 68.55.J–, 81.10.–h

**DOI:** 10.1088/1674-1056/adcb23 **CSTR:** 32038.14.CPB.adcb23

## 1. Introduction

AlN as a typical representative group III-nitride semiconductors boasts a wide direct energy bandgap of 6.2 eV, a high thermal conductivity, a high breakdown voltage, and a large piezoelectric constant, which makes it an ideal choice for deep ultraviolet light emitting diodes (DUV-LEDs) and power electronics.[1–8] In recent years, in order to improve the luminous efficiency of DUV-LEDs, the AlGaN quantum wells grown on large misoriented AlN/sapphire substrates,[9,10] lateral-polarity structure,[11] "Ni sacrifice" high-reflectivity p-electrodes,[12] and ultrathin tunneling junctions[13] have been optimized to some extent. For power electronics, the AlN-based metal–semiconductor field-effect transistor with breakdown voltages exceeding 2 kV have been fabricated on AlN single crystal substrate.[14] The oxygen-enriched fast thermal annealing technique can improve the rectification ratio of AlN-based Schottky barrier diode to 107, the breakdown voltage exceeds 1150 V, and still maintains a low on-resistance.[15]

The epitaxy growth methods of AlN films include metal organic chemical vapor deposition (MOCVD), hydride vapor phase epitaxy (HVPE), and molecular beam epitaxy (MBE).[16] The MBE offers unique advantages owing to its ultra-clean and ultra-high-vacuum environment, which effectively minimizes parasitic reactions and hydrogen passivation effects usually observed in MOCVD reactors. MBE systems allow precise control of rapid shutter opening and closing, enabling the realization of complex structures and sharp heterointerfaces.[17,18] The first challenge for homoepitaxy on an AlN template is obtaining a clean surface. Some $Al_xO_yN_z$-based materials on the surface possess high bond energies, making their *in-situ* removal problematic.[19–21] By removing these oxides containing Al *in situ*, to optimize the morphology of AlN films. The second challenge is that the growth mode of AlN is more difficult to control. The growth mode of AlN is characterized by N-rich, slightly Al-rich, and excessive Al-rich, depending on the Al supply.[22,23] Consequently, the Al/N ratio influences the quality of AlN films significantly. AlN films grown in the N-rich region exhibit a rough 3 dimensional (3D) morphology and poor crystal quality. Conversely, films grown in the slightly Al-rich region feature a smoother morphology and improved crystal quality. However, excessive Al-rich growth leads to the formation of numerous metal droplets on the growth front.[24] To circumvent the formation of Al droplets, researchers have employed some methods. The high-temperature desorption removes excessive Al droplets effectively,[21,25] but this method exceeds the growth temperature range of conventional MBE. The N radical beam irradiation method reacts with the surface-enriched droplets to form crystals.[26] And the metal-modulated epitaxy (MME)

†Corresponding author. E-mail: pfshao@nju.edu.cn
‡Corresponding author. E-mail: kewang@nju.edu.cn

© 2025 Chinese Physical Society and IOP Publishing Ltd. All rights, including for text and data mining, AI training, and similar technologies, are reserved.

method has been utilized.[27] For instance, Burnham *et al*. used the MME method to enhance lateral growth and eliminate excessive Al droplets.[28] The third challenge is that a significant number of surface pits have been commonly observed.[29] Nakajima *et al*. demonstrated that pit density strongly depended on the residual impurities of the MBE chamber.[30]

In this work, we systematically investigate the growth of AlN films over a broad range of growth temperatures and Al fluxes. For a usual MBE system, the growth temperature is usually design-limited, and cannot offer enough heat to substrates. Consequently, AlN epilayers grown at low temperature range either show Al droplets and pits when it is metal rich, due to the low migration rate of Al atoms, or show very rough surface when metal is not enough. By elevating the growth temperature, such a difficulty can be effectively overcome, and we were able to grow AlN films with much improved surface morphology and obtained step flow growth mode without any Al droplets and pits.

## 2. Experimental procedures

The morphology and defect characteristics of the films were analyzed using atomic force microscopy (AFM) and cathodoluminescence (CL) spectroscopy, coupled with scanning electron microscopy (SEM). All experiments were conducted using RIBER Compact 21 MBE system equipped with sources for Al, Ga, In, and a nitrogen plasma. The samples were grown on 4.5-μm thick C-plane AlN/sapphire templates fabricated via MOCVD. The nitrogen plasma was maintained at a flow rate of 0.7 standard cubic centimeters per minute (SCCM) and a radio frequency power of 450 W. *Ex-situ* cleaning of the samples was similar to the procedure described by Lee *et al*.[25] *In-situ* cleaning of the AlN template was carried out in the MBE growth chamber using thermal deoxidation at 900 °C for 10 min. The growth temperatures were monitored using pyrometers. The evolution of the AlN template surface was tracked by reflection high-energy electron diffraction (RHEED) using a charge coupled device camera and a frame collector.[31]

As shown in Figs. 1(a)–1(d), with the substrate temperature is increased from 600 °C to 900 °C, the RHEED pattern transitioned from bright spotty to well-defined bright stripes. Then we conducted energy dispersive x-ray (EDX) test and we found that the high-temperature treated sample shows no oxygen enrichment at the interface of MOCVD-AlN and MBE-AlN, in contrast to the untreated samples, which showed oxygen enrichment, as shown in Figs. 1(e)–1(j). Which indicates the removal of thermally volatile oxygen atoms and their complexes from the surface.[21]

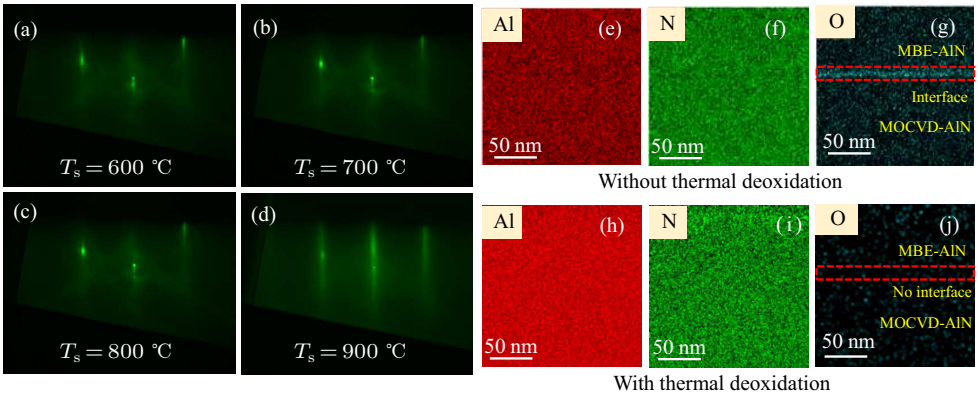



**Fig. 1.** Evolutions of the RHEED patterns of the AlN template taken along $[11\bar{2}0]$ direction during thermal deoxidation as the substrate temperature is increased from 600 °C to 900 °C [(a)–(d)] and the EDX spectroscopy of Al, N, and O elements near the interface of MBE AlN and MOCVD AlN [(e)–(j)].

## 3. Results and discussion

Figure 2(a) shows the variation of RHEED intensity signals with different Al flux for samples J, K, and L. The Al fluxes for samples J, K, and L are $3\times10^{-6}$ Torr (1 Torr = $1.33322\times10^{2}$ Pa), $2\times10^{-6}$ Torr, and $0.7\times10^{-6}$ Torr, respectively, with a growth temperature of 850 °C. The RHEED intensity of samples J and K decreases sharply when the Al shutter momentarily opens, whereas the RHEED intensity of sample L decreases gradually due to the lower Al flux. This suggests that at 850 °C, with an Al flux of $0.7\times10^{-6}$ Torr, the AlN epilayer growth likely results in a nitrogen-rich (N-rich) morphology. Within 600 s after the Al shutter was opened, approximately 2 monolayers (MLs) Al atomic layers and some Al droplets were formed on the surface of the AlN film (except for sample L). The presence of Al coverage reduces electron diffraction, leading to a decrease in RHEED intensity.[32,33] Then, the RHEED intensity stabilizes at its lowest level within about 600 s. After the Al shutter is turned off, the 2 MLs of Al coverage and Al droplets desorb.[34] Initially, Al droplets begin to desorb from the surface, corresponding to a time interval $\tau_1$. The values of $\tau_1$ for samples K and J are 80 s and 145 s, respectively. The absence of $\tau_1$ and $\tau_2$ for sample L is attributed to the lower Al flux, which prevents significant Al droplet accumulation during the growth

stage. Subsequently, the desorption of the 2 MLs of Al coverage occurs. The desorption time ($\tau_2$) for samples K and J is approximately 24 s, indicating that the desorption rate is more strongly influenced by the substrate temperature.[35]

Figure 2(b) displays the RHEED patterns during and after growth. During growth, the RHEED pattern transitions from bright spots to darker stripes and ultimately to a dark pattern as the Al flux increases. This change is attributed to the reduced electron diffraction resulting from excess Al atom coverage.[36,37] At the end of growth, the RHEED patterns exhibit increased brightness compared to the growth stage, as the desorption of Al atoms from the surface reduces coverage, enhancing diffraction and increasing brightness.[38]

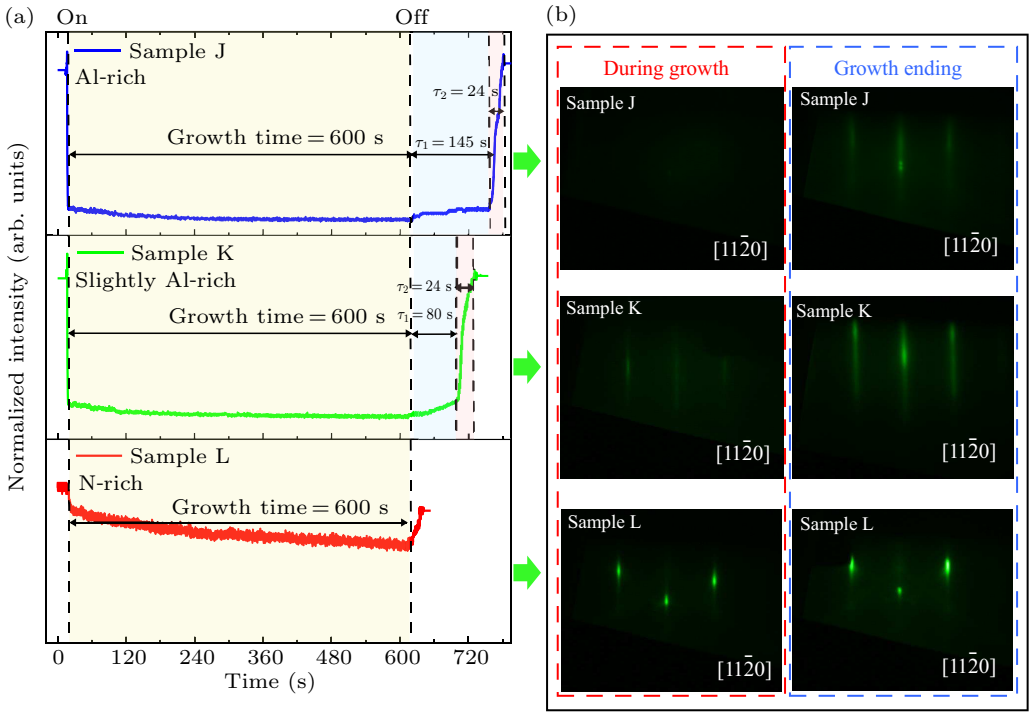



**Fig. 2.** Variations of RHEED intensity versus time (a) and the evolutions of RHEED patterns along the [10$\bar{1}$2] direction during growth and growth ending of samples J, K, L (b).

Figure 3 presents the AFM images of samples A–N (the corresponding optical microscope images are shown in Fig. S1 in the supporting information). At a growth temperature of 790 °C and an Al flux of $0.55\times10^{-6}$ Torr, a significant number of Al droplets are observed on the surface of sample A. This phenomenon is likely due to the inability of excessive Al droplets to thermally desorb at lower temperatures. When the Al flux is reduced to $0.32\times10^{-6}$ Torr, the Al droplets are no longer present on the surface of sample B. The root mean square (RMS) roughness of samples A and B is 1.19 nm and 1.3 nm in a 5 μm×5 μm area (mentioned below are 5 μm×5 μm), respectively. As the growth temperature increases to 820 °C and the Al flux is raised to $3\times10^{-6}$ Torr, a large number of Al droplets reappear on the surface of sample C. This may be attributed to the combined effects of lower temperature and high Al flux, which hinder the thermal desorption of Al droplets. The RMS roughness of sample C is 2.9 nm. Upon reducing the Al flux to $2\times10^{-6}$ Torr, the density of Al droplets on the surface of sample D decreases, and the RMS roughness is reduced to 1.25 nm. With a further decrease in the Al flux to $1\times10^{-6}$ Torr, sample E exhibits a step-flow morphology with no Al droplets or pits, and the RMS roughness is significantly reduced to 0.5 nm. As the Al flux is further reduced to $0.6\times10^{-6}$ Torr, sample F exhibits an N-rich morphology, characterized by a rough surface with numerous pits and cracks, leading to an increase in RMS roughness to 2.71 nm. At a higher growth temperature of 835 °C and an Al flux of $2.3\times10^{-6}$ Torr, a large number of Al droplets appear on the surface of sample G, resulting in RMS roughness of 2.37 nm. When the Al flux is subsequently reduced to $1.6\times10^{-6}$ Torr, the RMS roughness decreases to 0.39 nm, and a step-flow morphology emerges, with no Al droplets observed. As the Al flux is further reduced to $0.65\times10^{-6}$ Torr, the surface becomes extremely rough, with RMS roughness of 3.73 nm. At a growth temperature of 850 °C and an Al flux of $2\times10^{-6}$ Torr, sample K exhibits a large-area step-flow morphology, with RMS roughness as low as 0.36 nm. When the Al flux is increased to $3\times10^{-6}$ Torr or reduced to $0.7\times10^{-6}$ Torr, AlN epilayers grown in the Al-rich and N-rich regions exhibit RMS roughness values of 1.05 nm and 4.26 nm, respectively. At a growth temperature of 880 °C, sample M shows a step-flow morphology with fewer Al droplets compared to sample J, while sample N also shows a step-flow morphology without pits and Al droplets. The absence of Al droplets on the surface

of sample N is attributed to the higher growth temperature. As distinguished by the blue folded line in Fig. 3, according to the surface morphology of the samples A–N, they are roughly divided into the 3D rough region, the Al droplet region, and the step flow morphology region.

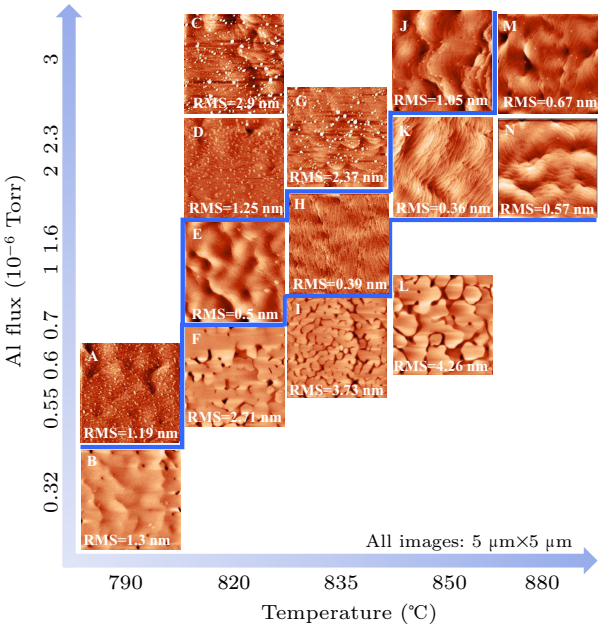



**Fig. 3.** The 5 μm×5 μm AFM images of the surface morphology evolutions as the substrate temperatures and Al flux vary for the sample A–N grown by MBE.

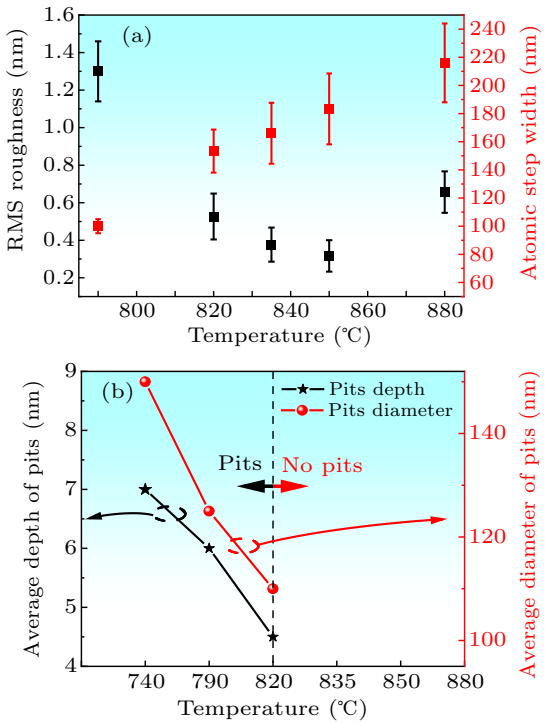



**Fig. 4.** The RMS roughness in a 5 μm×5 μm area and atomic step width (a), average depth and average diameter (b) for pits of samples at different growth temperatures and Al fluxes.

Figure 4(a) shows the RMS roughness and atomic step width for samples grown at different temperatures and Al fluxes. The average atomic step width increases from 100 nm to 214 nm as the growth temperature rises from 790 °C to 880 °C. It demonstrates that temperature is a critical factor, which strongly affects the surface morphology of MBE AlN epilayer. The migration capability of Al adatoms on the AlN surface enhanced by the higher growth temperatures, resulting in smooth surfaces with wider atomic steps.[39] Increasing the growth temperature to 850 °C improves RMS roughness to 0.36 nm. As shown in Fig. 4(b), both the average depth and diameter of the surface pits decrease progressively with increasing temperature. The detail of AlN epilayers grown at 740 °C are shown in Fig. S2. It is worth that the pits disappear as increasing growth temperature above 820 °C owing to the enhanced migration of Al atoms in the AlN growth front.

Figure 5 presents the SEM images [(a)–(d)] and the corresponding CL mappings [(a′)–(d′)] of the AlN template, and samples B, L, J, and K. In the high-temperature region, the slightly Al-rich morphology exhibits a flatter surface, as seen in the inset AFM image, while the N-rich and excessive Al-rich regions display rougher surfaces or Al droplets. Figure 5(a) shows that sample B, grown at a lower temperature, has a rough surface with several pits. CL is employed to detect defects by utilizing the luminescence generated when an electron beam impinges on the semiconductor sample. The CL signal originates from the energy released by electrons transitioning between the conduction and valence bands. Defects within the material alter the local luminescence energy, creating contrast that allows differentiation between normal material and defect sites.[40] As shown in Fig. 5(c′), the luminescence from sample K, grown in the slightly Al-rich region, is more uniform, with significantly fewer defects compared to the other samples. In contrast, sample J, grown in the excessive Al-rich region, exhibits dark circles corresponding to the position of Al droplets, as evidenced by the SEM image in Fig. 5(d). The SEM and CL mappings for samples B and L also correlate directly, with the defects in each sample producing luminescence distinct from that of the normal material. AlN films grown in the slightly Al-rich condition at high-temperature exhibit superior crystal quality with lower defect density.

Figure 5(e) shows the room-temperature CL spectra of the AlN template, sample B, sample L, sample J, and sample K in the ultraviolet (UV) region. The electron beam with an incident energy of 5 keV was used to excite the samples, ensuring that electron–hole pairs were generated exclusively within the homoepitaxial layers. The spectrometer was operated with a grating blazed at 500 nm and 300 grooves/mm, yielding a spectral resolution of 0.008 eV for a slit width of 0.1 mm. A peak of near-band-edge luminescence is observed at 208 nm (5.9 eV), corresponding to the AlN near-band-edge emission. In addition, a luminescence peak at 318 nm (3.89 eV) is identified. This peak is attributed to oxygen-related defects in AlN, consistent with data reported by Youngman *et al.*[41–43]

Both the AlN template and the low-temperature grown sample B exhibit much higher 320-nm band luminescence, indicating much more oxygen-related defects. Conversely, the high-temperature-grown samples show lower peak intensities, with sample K having the lowest, suggesting the lowest defect density associated with oxygen impurities.

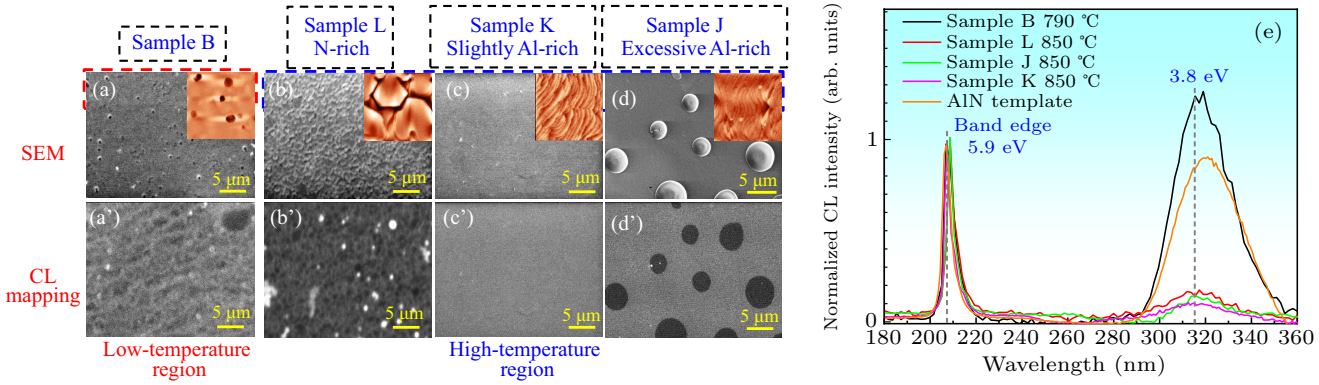



**Fig. 5.** The AFM images (inserts: 2 μm×2 μm) in the SEM images, SEM images [(a)–(d)], the CL- mappings [(a′)–(d′)] and the room temperature CL spectra (e) of AlN template, sample B, sample L, sample J, and sample K.

The high-resolution TEM cross section images for slightly Al-rich sample shows in Fig. 6. In Fig. 6(a), the homogeneous epitaxial interface between MOCVD-AlN and MBE-AlN was not observed indicating that the high temperature treatment, which performed before MBE epitaxial AlN, can play a critical role in achieving a better homogeneous epitaxial AlN films. Figure 6(b) demonstrates that sample K has a relatively clear and regular atomic arrangement, and similarly no growth interface is found, which fully indicates that sample K achieves a superior epitaxial growth. The above illustrates that high-temperature heat treatment of MOCVD-AlN improves the interfacial quality and enhances the orderliness of atomic arrangement.

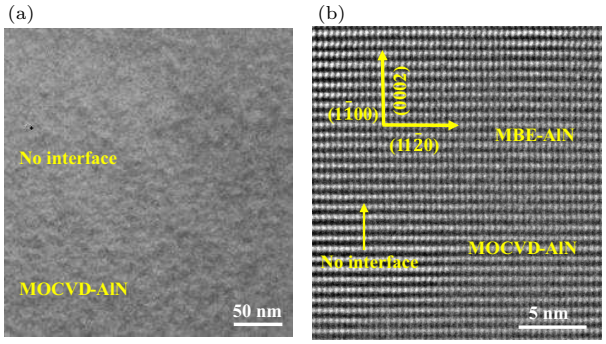



**Fig. 6.** TEM analysis of near the MBE AlN/MOCVD AlN interface of sample K. (a) The cross-sectional many-beam dark-field image along the [0002] direction near the MBE-AlN/MOCVD-AlN interface, (b) high resolution HAADF-STEM image in [10$\bar{1}$2] AlN zone axis of an interface between the MBE-AlN and MOCVD-AlN.

Based on the characterization results of samples A–N, the growth diagram was summarized. In the growth diagram, there are three regions: excessive Al-rich, slightly Al-rich, and N-rich as shown in Fig. 7. This is similar to the growth behavior observed in GaN, however, the growth temperature for GaN is lower than that for AlN.[23,39,44] The boundaries of the growth regions are indicated by the black lines, which are identified based on the results of RHEED patterns, surface morphologies and defect analysis of above. In different growth regions, the thickness of surface coverage of Al adatoms is different. In the excessive Al-rich region, due to the excess Al supply, it is usually supposed to be much more than 2 MLs[34] Al adatoms on the growth front causing the formation of Al droplets as shown in Fig. 3. In the slightly Al-rich region, Al supply is sufficient and it is supposed to be about 2-MLs Al adatoms on the growth front. In the N-rich regions, compared with the amount of the active nitrogen, Al supply is not sufficient in a range and it is supposed to be less than one monolayer of Al adatoms on the growth front.

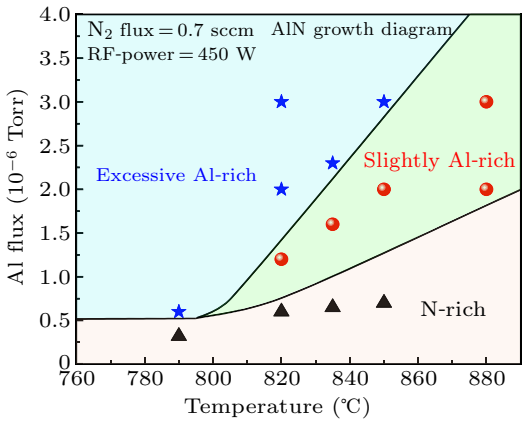



**Fig. 7.** The AlN growth diagram with the three regions: excessive Al-rich, slightly Al-rich, and N-rich for the AlN epilayers grown by PA-MBE.

Due to the Al adatoms desorption rate strongly depends on the growth temperature. In the temperature range below 790 °C, the Al droplet desorption rate is low as the Al flux changes and the growth region can easily change directly from N-rich to excessive Al-rich, because the Al flux window in the slightly Al-rich region is extremely narrow. In the temperature range of 790 °C–835 °C, the Al flux window in the slightly Al-rich region, becomes wider as the Al desorption rate becomes higher with increasing growth temperature. The slightly Al-rich region can be reached by adjusting the Al flux. However, above 835 °C, the Al desorption rate is very high, and therefore a large supply of Al is required to ensure that the growth front

is covered with 2 MLs of Al atoms to maintain the slightly Al-rich condition. The growth diagram can establish a foundation for the subsequent epitaxial growth of complex device structures.

## 4. Conclusions

In summary, we have conducted MBE-based epitaxial growth of homogeneous AlN epilayers across a wide range of temperatures and Al fluxes. By increasing the growth temperature beyond a usual MBE system can reach, we achieved significant improvement in the surface morphology and crystalline quality of the AlN films. The step-flow morphology AlN epilayers without Al droplet and pits have been obtained. Elevated temperatures are crucial for promoting the thermal desorption of Al droplets and enhancing the mobility of Al atoms. Furthermore, being able to reasonably match the Al flux at higher growth temperatures is also the key to obtain step-flow morphology of AlN epilayers. The CL measurements indicate that high temperature growth is necessary to suppress the impurity incorporation and defect generation, particularly those related to oxygen impurities in the AlN epilayers. After systematically investigating the influence of Al flux and growth temperature on AlN film morphology, a comprehensive growth diagram of MBE AlN has been obtained.

## Acknowledgements

Project supported by the Innovation Program for Quantum Science and Technology (Grant No. 2021ZD0303400), the National Key Research and Development Program of China (Grant Nos. 2022YFB3605602 and 2024YFE0205000), the Natural Science Foundation of Jiangsu Province, China (Grant No. BK20243037), and the Jiangsu Special Professorship, Collaborative Innovation Center of Solid-state Lighting and Energy-saving Electronics, Postdoctoral Fellowship Program of CPSF (Grant No. GZC20231098).

## References

[1] Taniyasu Y, Kasu M, Makimoto T 2006 *Nature* **441** 325
[2] Li X H, Detchprohm T, Kao T T, *et al.* 2014 *Appl. Phys. Lett.* **105** 141106
[3] Melo E G and Alayo M I 2015 *Photonics and Nanostructures-Fundamentals and Applications* **14** 35
[4] Wang X P, Fabi G, Chaudhuri R, Hickman A, Asadi M J, Nomoto K, Xing H G, Jena D, Farina M and Hwang J C M 2022 *Appl. Phys. Lett.* **120** 012103
[5] Qi M, Li G, Ganguly S, Zhao P, Yan X, Verma J, Song B, Zhu M, Nomoto K and Xing H G 2017 *Appl. Phys. Lett.* **110** 063501
[6] Collazo R, Mita S, Xie J, Rice A, Tweedie J, Dalmau R and Sitar Z 2011 *Phys. Status Solidi C* **8** 2031
[7] Wang C, Gao X D, Li D D, Chen J J, Chen J F, Dong X M, Wang X D, Huang J, Zeng X H and Xu K 2024 *Chin. Phys. B* **32** 026802
[8] Su Z L, Li Y F, Hu X T, Song Y M, Deng Z, Ma Z G, Du C H, Wang W X, Jia H Q, Jiang Y and Chen H 2024 *Chin. Phys. B* **33** 117801
[9] Sun H D, Mitra S, Subedi R C, Zhang Y, Guo W, Ye J C, Shakfa M K, Ng T K, Ooi B S, Roqan I S, Zhang Z H, Dai J N, Chen C Q and Long S B 2019 *Adv. Funct. Mater.* **29** 1905445
[10] Xu H Q, Jiang J A, Sheikhi M, Chen Z Y, Hoo J, Guo S P, Guo W, Sun H D and Ye J C 2019 *Superlattices and Microstructures* **129** 20
[11] Guo W, Sun H D, Torre B, Li J M, Sheikhi M, Jiang J A, Li H W, Guo S P, Li K H, Lin R H, Giugni A, Di Fabrizio E, Li X H and Ye J C 2018 *Adv. Funct. Mater.* **28** 1802395
[12] Ding Y, Zhou S, Zhuang Z, Sang Y, Yu J, Xu F, Huang J, Xu W, Tao T, Zhi T, Lu H, Huang K, Zhang R and Liu B 2023 *Opt. Express* **31** 24
[13] Zhou S, Liao Z, Sun K, Zhang Z, Qian Y, Liu P, Du P, Jiang J, Lv Z and Qi S 2024 *Laser Photon. Rev.* **18** 2300464
[14] Da B, Herath Mudiyanselage D, Wang D, He Z and Fu H 2024 *Appl. Phys. Express* **17** 104002
[15] Cao H, Nong M, Liu T, Garcia GI, Liu Z, Tang X, Kumar M, Sarkar B, Wu Y and Li X 2025 *Trans. Electron Dev.* **72** 1533
[16] Zhao L, Yang K, Ai Y, Zhang L, Niu X, Lv H and Zhang Y 2018 *J. Mater. Sci.: Mater. Elect.* **29** 13766
[17] Nakarmi M L, Cai B, Lin J Y and Jiang H X 2012 *Phys. Status Solidi A* **209** 126
[18] Wu Y Z, Liu B, Li Z H, Tao T, Xie Z L, Xiu X Q, Chen P, Chen D J, Lu H, Shi Y, Zhang R and Zheng Y D 2019 *J. Cryst. Growth* **506** 30
[19] Rice A, Collazo R, Tweedie J, Dalmau R, Mita S, Xie J and Sitar Z 2010 *J. Appl. Phys.* **108** 043510
[20] Dycus J H, Mirrielees K J, Grimley E D, Kirste R, Mita S, Sitar Z, Collazo R, Irving D L and James M 2017 *Microscopy & Microanalysis* **23** 1444
[21] Cho Y J, Celesta S C, Kevin L, Mingli G, Nomoto K, Masato T, Schowalter L J, Muller D A, Jene D and Huili G X 2020 *Appl. Phys. Lett.* **116** 172106
[22] Heying B, Averbeck R, Chen L F, Haus E, Riechert H and Speck J S 2000 *J. Appl. Phys.* **88** 1855
[23] Li Z H, Shao P F, Shi G J, Wu Y Z, Wang Z P, Li S Q, Zhang D Q, Tao T, Xu Q J, Xie Z L, Ye J D, Chen D J, Liu B, Wang K, Zheng Y D and Zhang R 2022 *Chin. Phys. B* **31** 018102
[24] Kaneko M, Hirai K, Kimoto T and Suda J 2020 *Appl. Phys. Express* **13** 025503
[25] Lee K, Cho Y J, Schowalter L J, Toita M, Xing H G and Jena D 2020 *Appl. Phys. Lett.* **116** 262102
[26] Yamaguchi T, Uematsu N and Araki T 2013 *J. Cryst. Growth* **377** 123
[27] Burnham S D, Henderson W and Doolittle W A 2008 *Phys. Status Solidi C* **5** 1855
[28] Burnham S D, Namkoong G, Lee, K K and Doolittle W A 2007 *Journal of Vacuum Science & Technology B Microelectronics & Nanometer Structures* **25** 3
[29] Shao P F, Li S Q, Li Z H, Zhou H, Zhang D Q, Tao T, Yan Y, Xie Z L, Wang K, Chen D J, Liu B, Zheng Y D, Zhang R, Lin T, Wang L and Hirayama H 2022 *J. Phys. D: Appl. Phys.* **55** 364002
[30] Nakajima A, Furukawa Y, Koga S and Yonezu H 2004 *J. Cryst. Growth* **265** 351
[31] Li Z H, Shao P F, Wu Y Z, Shi G J, Tao T, Xie Z L, Chen P, Zhou Y G, Xiu X Q, Chen D J, Liu B, Wang K, Zheng Y D, Zhang R, Lin T, Wang L and Hirayama 2021 *Jpn. J. Appl. Phys.* **60** 075504
[32] Adelmann C, Brault J, Mula G, Daudin B, Lymperakis L and Neugebauer J 2003 *Phys. Rev. B* **67** 165419
[33] Gallinat C S, Koblmueller G, Brown J S and Speck J S 2007 *J. Appl. Phys.* **102** 064907
[34] Liu H, Shao P F, Chen S L, Tao T, Yan Y, Xie Z L, Liu B, Chen D J, Lu H, Zhang R and Wang K 2024 *Chin. Phys. B* **33** 106801
[35] Li Z H, Shao P F, Shi G J, Wu Y Z, Wang Z P, Li S Q, Zhang D Q, Tao T, Xu Q J, Xie Z L, Ye J D, Chen D J, Liu B, Wang K, Zheng Y D and Zhang R 2022 *Chin. Phys. B* **31** 018102
[36] Tsai J K, Lo I, Chuang K L, Tu L W, Huang J H, Hsieh C H and Hsieh K Y 2004 *J. Appl. Phys.* **95** 460
[37] Okumura H, Balakrishnan K, Hamaguchi H, Koizumi T and Yoshida S 1998 *J. Crystal Growth* **189–190** 364
[38] Koblmüller G, Brown J, Averbeck R, Riechert H, Pongratz P and Speck J S 2005 *Jpn. J. Appl. Phys.* **44** 906
[39] Pan J H, Wang X Q, Chen G, Liu S T, Feng L, Xu F J, Tang N and Shen B 2011 *Chin. Phys. Lett.* **28** 068102
[40] Zhao H, Zhang R, Xie Z L, Liu B, Xiu X Q, Lu H, Li L, Liu Z H, Jiang R L and Han P 2008 *J. Semicond.* **29** 1184
[41] Koppe T, Hofsass H and Vetter U 2016 *Journal Luminescence* **178** 267
[42] Tang X, Hossain F, Wongchotigul K and Spencer M G 1998 *Appl. Phys. Lett.* **72** 1501
[43] Youngman R A and Harris J H 1990 *Journal American Ceramic Society* **73** 3238
[44] Keller S, Keller B P, Wu Y F, Heying B, Kapolnek D, Speck S, Mishra U K and DenBaars S P 1996 *Appl. Phys. Lett.* **68** 1525